Supplement of Atmos. Chem. Phys., 24, 1193–1212, 2024
https://doi.org/10.5194/acp-24-1193-2024-supplement

Atmospheric Chemistry and Physics
Open Access
EGU

Supplement of

Source apportionment of $PM_{2.5}$ in Montréal, Canada, and health risk assessment for potentially toxic elements

Nansi Fakhri et al.

Correspondence to: Charbel Afif (charbel.afif@usj.edu.lb) and Patrick L. Hayes (patrick.hayes@umontreal.ca)

SUPPLEMENTARY INFORMATION

Table S1: Values of the cancer slope factor (CSF) and inhalation unit risk (IUR).

	Cancer slope factor (CSF) (kg·day/mg)			Inhalation unit risk (IUR) (m^3/mg)
	Dermal	**Ingestion**	**Inhalation**	
Co			9.8	9
Cr(VI)	20	0.5	41	84
Ni			0.84	0.26
V				8.3
Cd			6.3	1.8
Pb	0.0085	0.0085	0.042	0.000012

Table S2: Displacement error estimation and mapping of bootstrap factors to constrained factors for the PMF model.

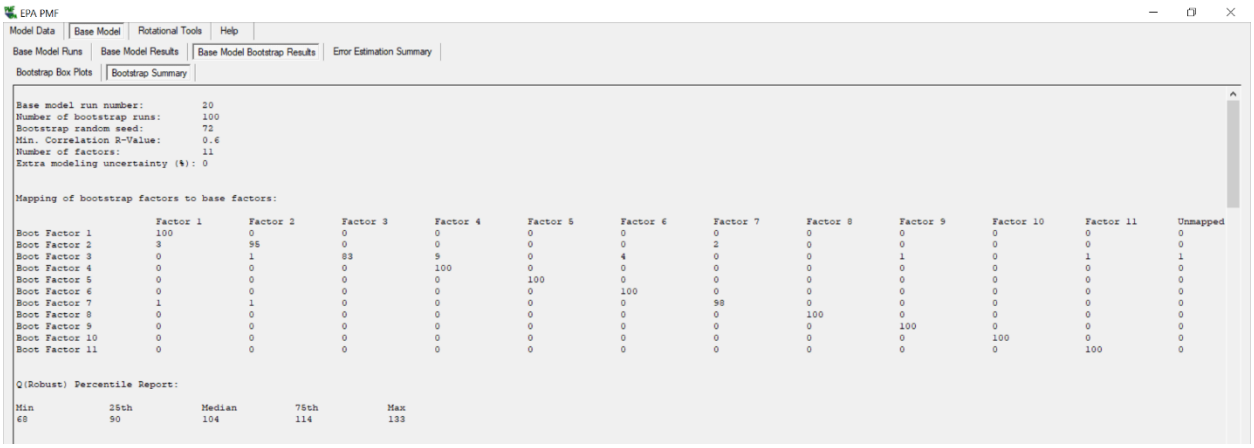

In order to reduce the range of the meaningful number of factors, two parameters was calculated: the maximum individual mean (IM) and the maximum individual standard deviation (IS) where (Lee et al., 1999):

$$IM = \max_{j=1\ldots m}\left(\frac{1}{n}\sum_{i=1}^{n} r_{ij}\right) \quad \text{and} \quad IS = \max_{j=1\ldots m}\left(\sqrt{\frac{1}{n-1}\sum_{i=1}^{n}(r_{ij} - \bar{r}_j)^2}\right)$$

$$r_{ij} = \frac{e_{ij}}{s_{ij}}$$

When the number of factors increases to a critical value, IM and IS will show a drastic drop.

Graphical representations of the IM and IS (**Fig. S1**) revealed a steady drop in their values as the number of factors increased and a stabilization starting with the 11-factor solution. Moreover, a 12-factor solution resolved a phantom factor that could not be definitively linked to a particular source, while a 10-factor solution consolidated two sources into a single factor (Esmaeilirad et al., 2020).

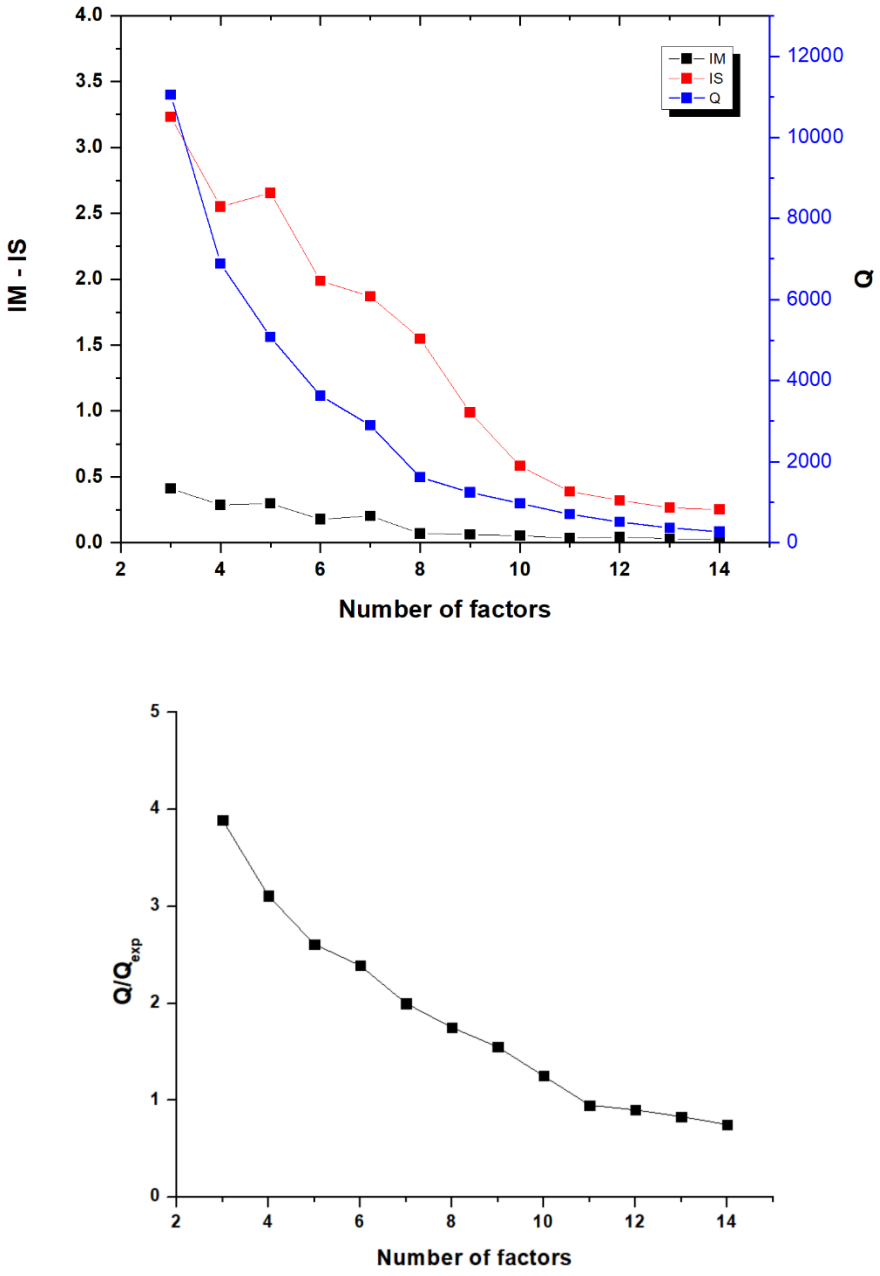

Fig. S1: IM, IS and Q-values for MTL site.

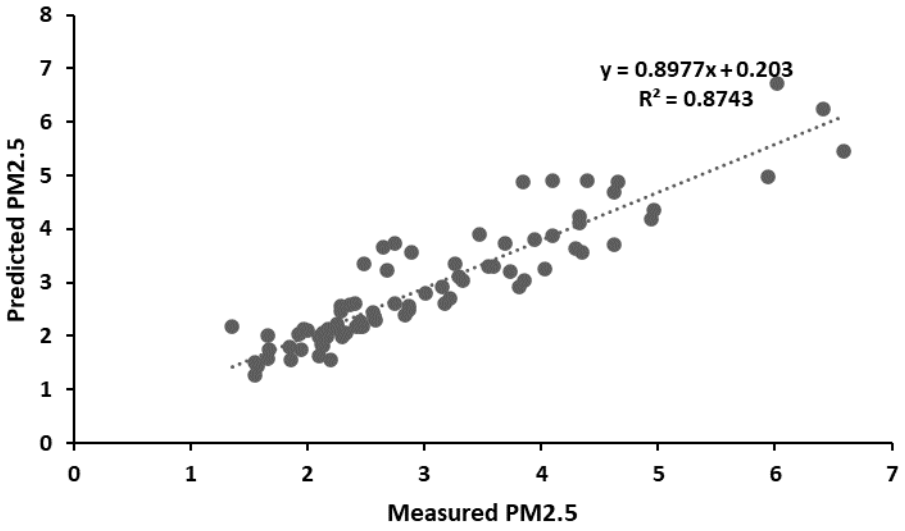

Fig. S2: Measured versus predicted $PM_{2.5}$ concentrations.

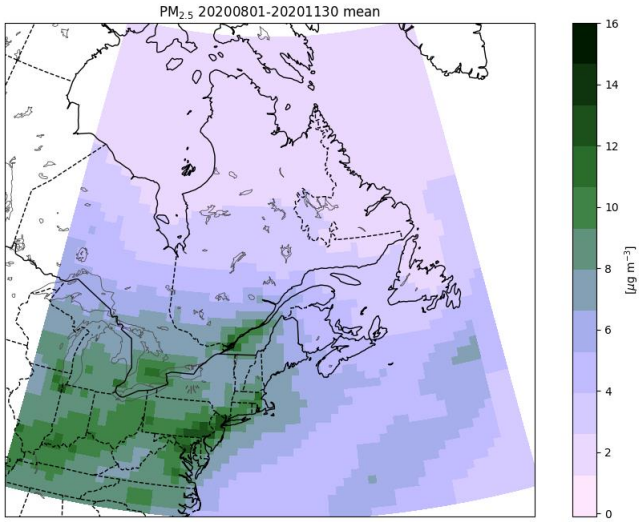

Fig. S3: Mean concentrations of $PM_{2.5}$ from the base case 0.5x0.625 nested GEOS-Chem simulation.

Evaluation of GEOS-Chem against measurements

The model performance was evaluated for $PM_{2.5}$, SO_4^{2-}, NO_3^-, NH_4^+, OC and EC and the results are summarized in **Table S3**. The metrics used for the evaluation were: Pearson's correlation coefficient (R), mean error (ME), normalized mean error (NME), mean bias (MB), and normalized mean bias (NMB). ME, NME, MB, and NMB are calculated following the Eqs. 1-4, where x_i indicates the model predictions and y_i indicates the observed data for a given month and station, both as daily averages, and N is the number of model-observation pairs:

$$\mathrm{ME} = \frac{1}{\mathrm{N}}\sum_{\mathrm{i}=1}^{\mathrm{N}} |\mathrm{x_i} - \mathrm{y_i}| \qquad \text{(Eq. 1)}$$

$$\mathrm{NME} = \frac{\sum|\mathrm{x_i}-\mathrm{y_i}|}{\sum \mathrm{y_i}} \cdot 100 \qquad \text{(Eq. 2)}$$

$$\mathrm{MB} = \frac{1}{\mathrm{N}}\sum_{\mathrm{i}=1}^{\mathrm{N}} \mathrm{x_i} - \mathrm{y_i} \qquad \text{(Eq. 3)}$$

$$\mathrm{NMB} = \frac{\sum(\mathrm{x_i}-\mathrm{y_i})}{\sum \mathrm{y_i}} \cdot 100 \qquad \text{(Eq. 4)}$$

Table S3: Evaluation of the GEOS-Chem base case simulation vs measurements from our measurement site.

Pollutants	**R**	**ME**	**NME [%]**	**MB**	**NMB [%]**
$PM_{2.5}$ (μg m^{-3})	0.63	4.69	141.08	4.46	133.98
SO_4^{2-} (μg m^{-3})	0.24	0.43	77.14	0.18	32.39
NO_3^- (μg m^{-3})	0.56	0.30	107.92	0.11	40.95
NH_4^+(μg m^{-3})	0.46	0.23	89.09	0.15	57.08
OC (μg m^{-3})	0.76	0.89	51.46	0.11	41.02
EC (μg m^{-3})	0.57	0.16	58.84	0.01	2.89

We note that significant errors are expected due to the differences in spatial extent of the model resolution (0.5 degrees latitude by 0.625 degrees longitude) versus the observations (essentially a point measurement) as discussed by Schutgens et al. (2016). However, this bias is expected to affect all of the sensitivity simulations in a similar way and would not affect the relative differences between simulations that we use to help interpret the results of the PMF analysis. Furthermore, GEOS-Chem results have been previously used for source contribution analysis similar to the analysis presented in this study (Meng et al. 2019).

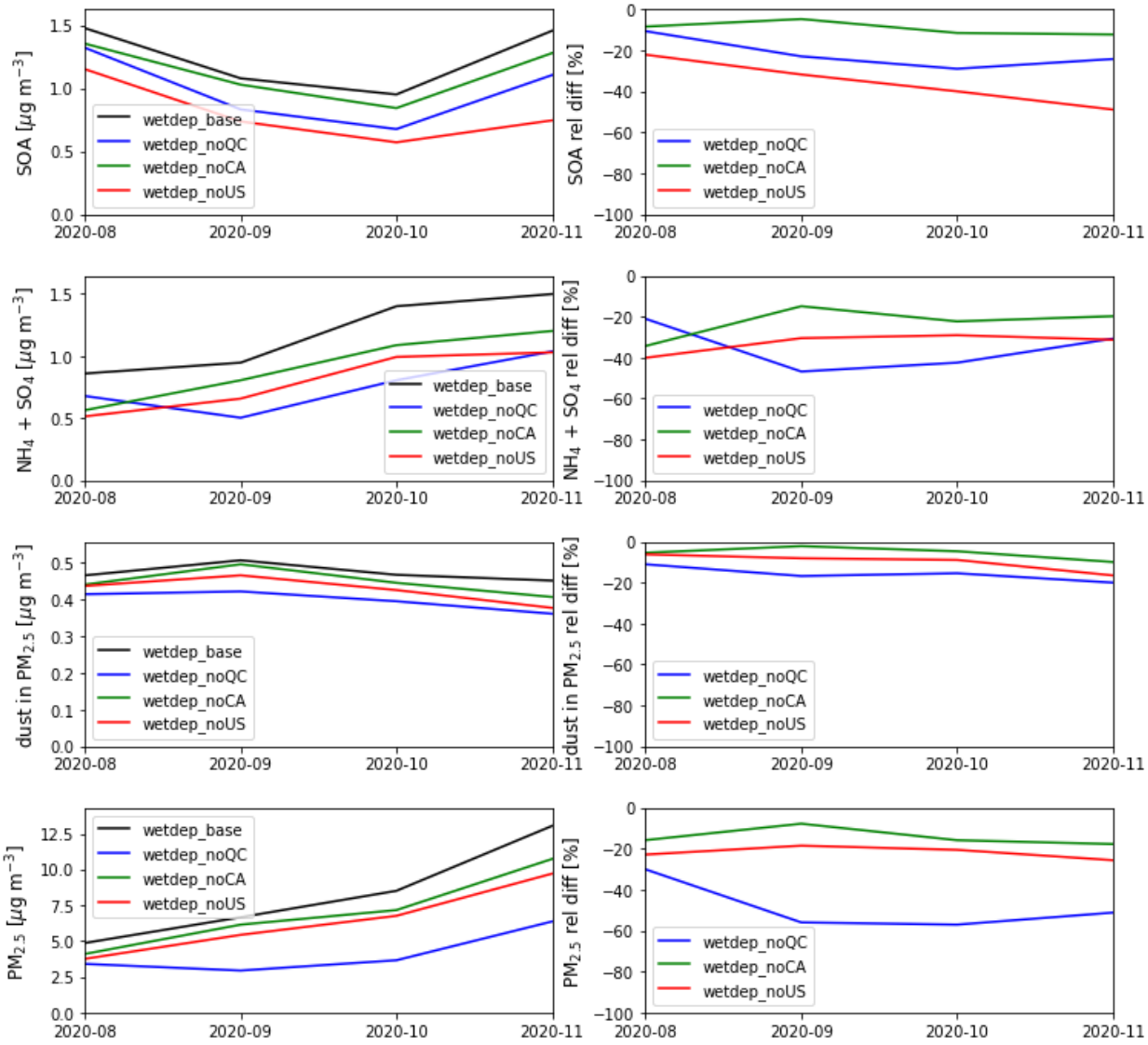

Fig. S4: GEOS-Chem simulations of (top) SOA, (middle 1) the sum of ammonium and sulfate concentrations, (middle 2) dust in $PM_{2.5}$, and (bottom) $PM_{2.5}$. The labels noQC, noCA, and noUS refer to simulations without anthropogenic emissions from Quebec, the rest of Canada, and the US, respectively.

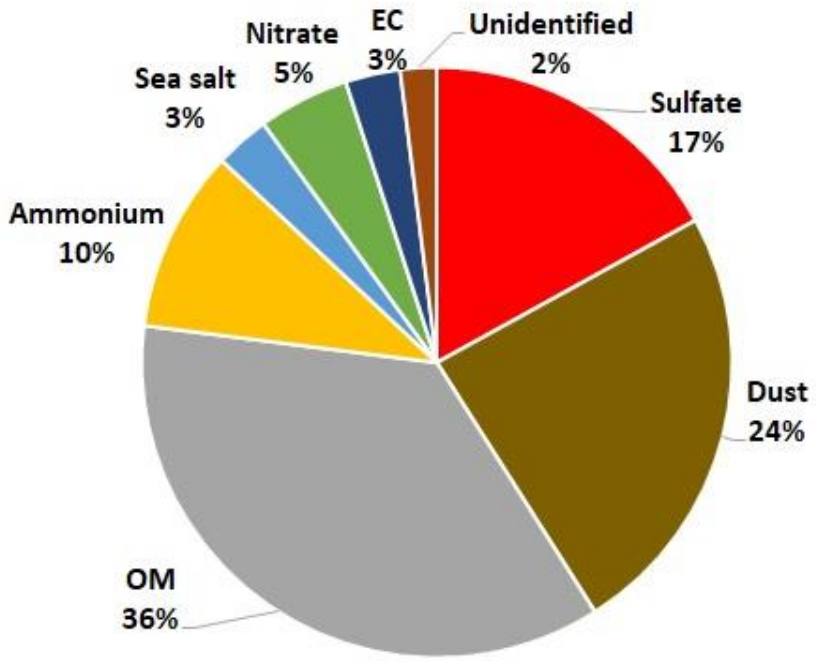

Fig. S5: Percent source contributions determined by chemical mass closure.

The indexes for the n-alkanes

Overall CPI and high CPI were calculated using the concentrations of n-alkanes following the Eq. 5 and 6 (Bray and Evans, 1961; Cooper and Bray, 1963; Fadel et al., 2021):

$$\text{Overall CPI} = \frac{\Sigma \text{ odd C15–C29}}{\Sigma \text{ even C16–C30}} \qquad \text{(Eq. 5)}$$

$$\text{High CPI} = \frac{\Sigma \text{ odd C25–C29}}{\Sigma \text{ even C26–C30}} \qquad \text{(Eq. 6)}$$

Biogenic sources emit larger amounts of odd carbon number alkanes than even carbon number alkanes, resulting in an Overall CPI greater than 6. Petrogenic emissions, on the other hand, have no carbon preference and have an Overall CPI value close to 1, whereas biomass burning has a value between 2 and 5 (Haque et al., 2019; Li et al., 2010; Fadel et al., 2021). When only the higher molecular weight n-alkanes are considered, anthropogenic sources have CPI values below 1.5, while biogenic sources have CPI values higher than 3 (Caumo et al., 2020; Kang et al., 2020).

Furthermore, wax n-alkane concentrations were used to assess the relative contributions of biogenic and anthropogenic sources. The concentrations of wax n-alkanes (WNA), in the C14 to C30 range, and its percentage (%WNA) were calculated using the following equations (Fadel et al., 2021):

$$\mathrm{WNA_n} = \mathrm{C_n} - 0.5(\mathrm{C_{n-1}} + \mathrm{C_{n+1}}) \qquad (\mathrm{Eq.}\,7)$$

$$\%\mathrm{WNA} = \frac{\sum \mathrm{WNA}}{\sum \mathrm{NA}} \times 100 \qquad (\mathrm{Eq.}\,8)$$

where C_n is the odd carbon congener, ΣWNA is the sum of wax n-alkane concentrations and ΣNA is the total concentration of n-alkanes. The %WNA value of 7.95±4.93% was indicative of smaller relative inputs from biogenic sources compared to the anthropogenic ones. Hence, the Overall CPI, High CPI and %WNA all appear to depict a similar picture of the anthropogenic origins of n-alkanes.

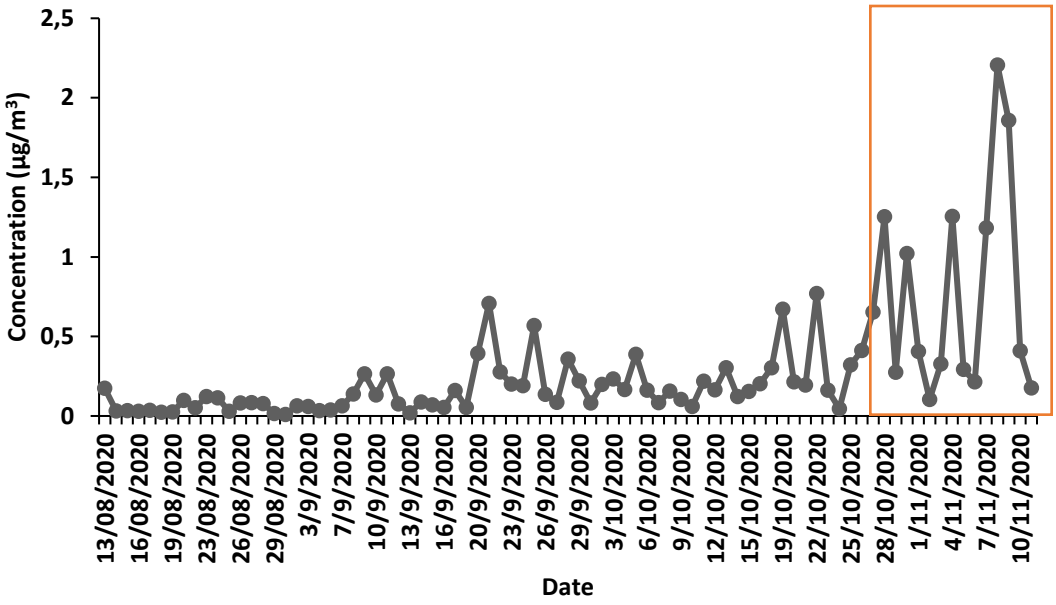

Fig. S6: The temporal variation of nitrate concentrations for the sampling period at the MTL site. The red box indicates the period (end of October and November) where the nitrate concentrations were higher in comparaison with the warmer months.

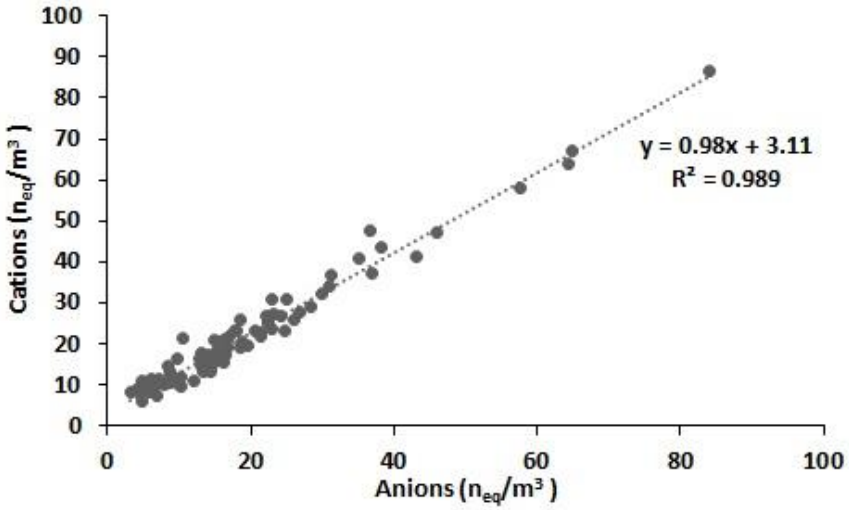

Fig. S7: Ion balance evaluation between the water-soluble ions (Cations: Na^+, Mg^{2+}, NH_4^+, K^+, Ca^{2+} and anions: SO_4^{2-}, NO_3^-, Cl^-).

Table S4: Species included in the PMF analysis.

Species	% of data below the DL	Species	% of data below the DL
OC	-	Levoglucosan	-
EC	-	7α[H]-21β[H]-Hopane	-
Na^+	-	Hexadecanoic acid	-
Cl^-	-	Octadecanoic acid	-
NH_4^+	-	C20	-
NO_3^-	-	C21	-
SO_4^{2-}	-	C24	-
Al	3	C25	-
Fe	1	C27	-
Ti	-	C29	-
Cu	4	Oxalic acid	-
Sb	3	Pinic acid	-
Cd	5	Cis-pinonic acid	-
Co	12		

Secondary organic carbon

While EC is derived only from combustion processes, organic carbon (OC) is produced by both primary and secondary sources. Several studies have estimated the contribution of secondary organic carbon (SOC) by employing the OC/EC minimum ratio method and the following equation (Castro et al., 1999; Shivani et al., 2019; Cesari et al., 2018; Calvo et al., 2008; Joseph et al., 2012).

$$SOC = OC_{total} - EC \times \left(\frac{OC}{EC}\right)_{min} \quad (Eq. 9)$$

In the first step, the OC/EC ratio is calculated for each sample, and $(OC/EC)_{min}$ is the minimum ratio observed in the samples. In this study, $(OC/EC)_{min}$ was 2.22. In the second step, the measured OC (OC_{total}) and EC for each sample are used with the minimum to calculate the SOC following the equation above.

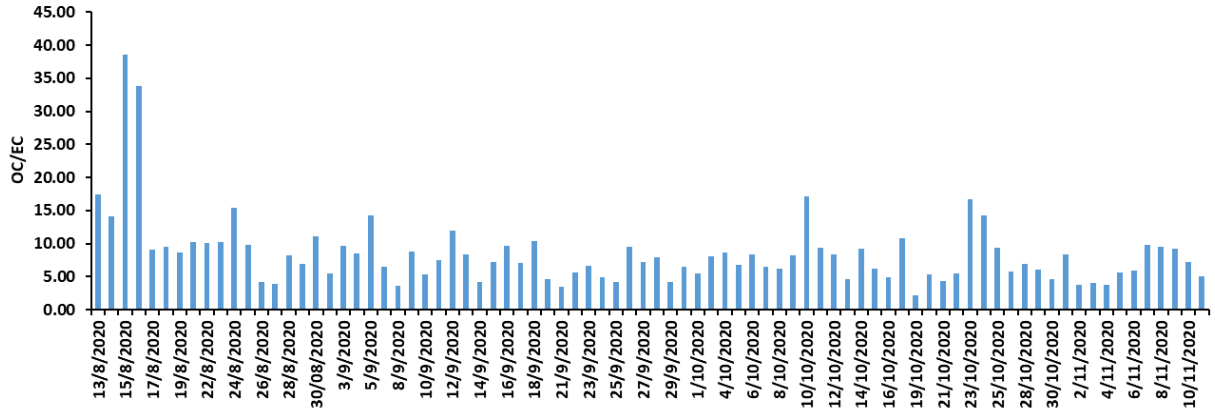

Fig. S9: The temporal variation of OC/EC ratio for the sampling period.

Pollution rose

The pollution roses in **Figure S10** displays the frequency of a given concentration of a factor as a function of wind direction. The wind data was taken from a nearby meteorological station at Montréal-Pierre Elliott Trudeau Airport. In general, the pollution rose plots are consistent with the identification of the factors proposed in the manuscript.

The traffic exhaust and road dust factors show similar polar plots with the highest concentrations of these factors being observed when the wind is from the southern and western directions. The observations of high factor concentrations with winds from these directions is expected given that major highways (Autoroutes 15 and 40) are located to the west and the south of the measurement

site, and winds from the south and west tend to have higher speeds facilitating transport. The road dust factor also exhibits some periods of very high concentrations when the wind is from the northeast, possibly due to the greater influence of very local emissions and surface streets.

In contrast, the biomass burning and crustal dust factors dust showed higher concentrations when winds were from the northeast. No major highways are in this direction. The biomass burning factor showed no trend with date during the campaign period. It is possible that this factor is related to certain food preparation activities such pizzerias and bagel bakeries that traditionally use wood ovens. Similarly, the crustal dust factor may be attributable to local construction activities, although further studies of the sources of these factors is needed. Interestingly, the cooking factor, unlike the biomass burning factor, shows little dependence on wind direction, which is reasonable given the measurement site is surrounded by residential neighborhoods and many restaurants.

The SIA and SOA factor both have similar dependences on wind direction with the highest concentrations tending to be observed when the wind is from the south and southwest. As already mentioned for the traffic-related factors above, winds from this direction can potentially transport aerosol and aerosol-precursors to the measurement site from major highways located to the south and southwest of the site. Alternatively, as discussed in the main text, GEOS-Chem modeling shows large transboundary contributions from the USA to these components. Thus, the wind blowing from the south may also correspond to large scale transport from south to north that increases the transboundary contribution to the SIA and SOA factors.

Both the biogenic SOA and plant wax factors exhibit high concentrations when winds are blowing from the northwest. In this direction is a major suburb of Montréal, Town of Mont-Royal, which contains a high density of trees relative to the rest of the metropolitan area. At the same time, we note that the biogenic SOA factor reaches moderately high concentrations for almost all wind

directions, suggesting the importance of regional formation, which is expected to be important for this factor.

The marine factor exhibits relatively high concentrations for multiple wind directions including from the west and southwest. Thus, the marine factor pollution rose resembles to some extent that of road dust. It is also notable that the marine factor exhibits its highest concentrations in November when minimum temperatures were below freezing, and some snowfall occurred. Thus, it is possible that is factor originates from road salt, although further work is needed to evaluate the contribution of road salt to $PM_{2.5}$ in Montréal.

Lastly, the industrial factor exhibits its highest concentration when winds are blowing from the west and north. Many major industries on the Island of Montreal are located to the northeast of the site (e.g., the Suncor Energy Refinery). Thus, the pollution rose for the industrial factor does not correspond to the location of these sources. This discrepancy may be explained by changes in wind direction upwind of the site, especially given that the distances to some of the largest potential emitters is approximately 10 km.

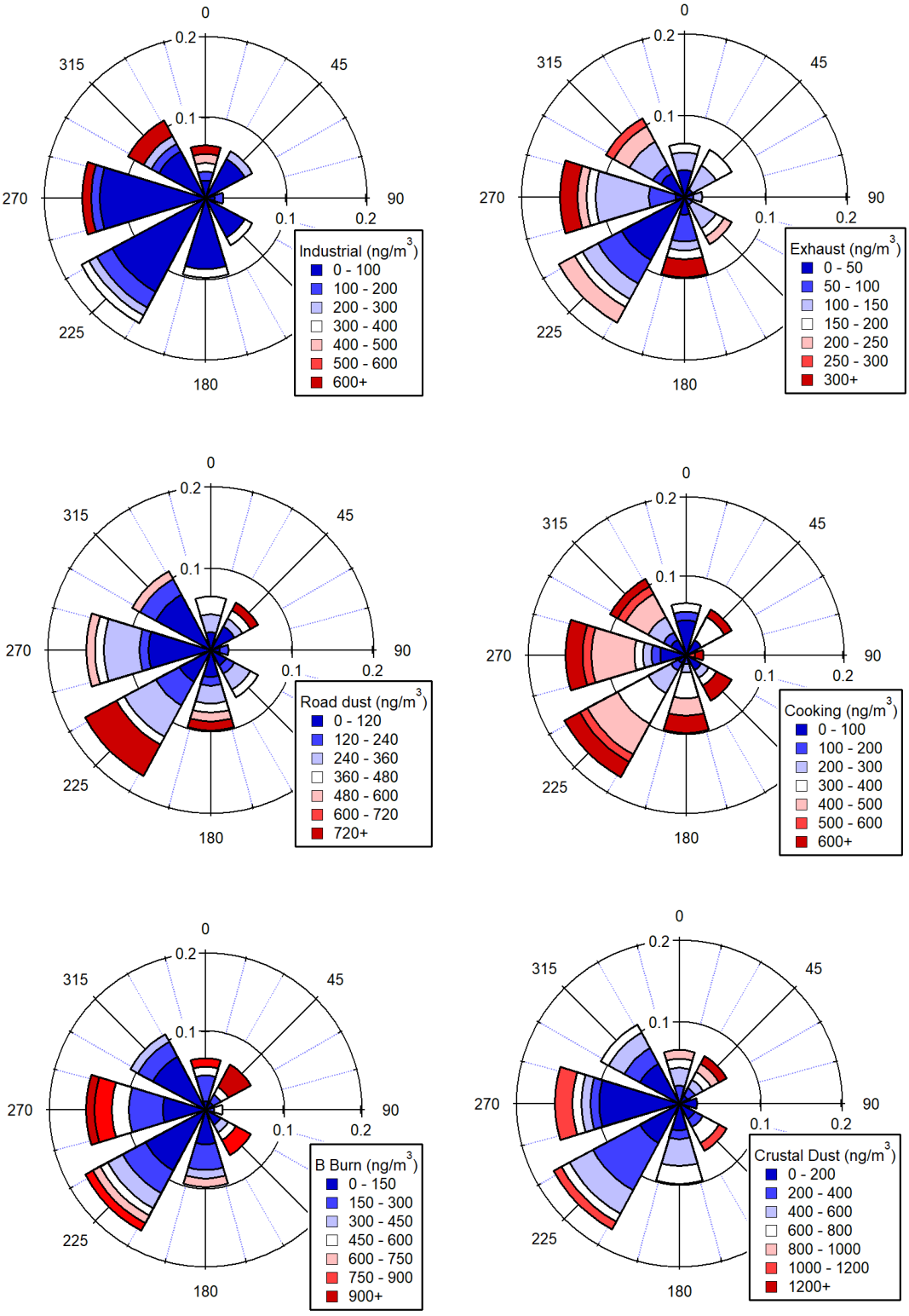

Fig. S10: Pollution rose plots for the PMF factors showing the frequency of a given concentration as function of wind direction.

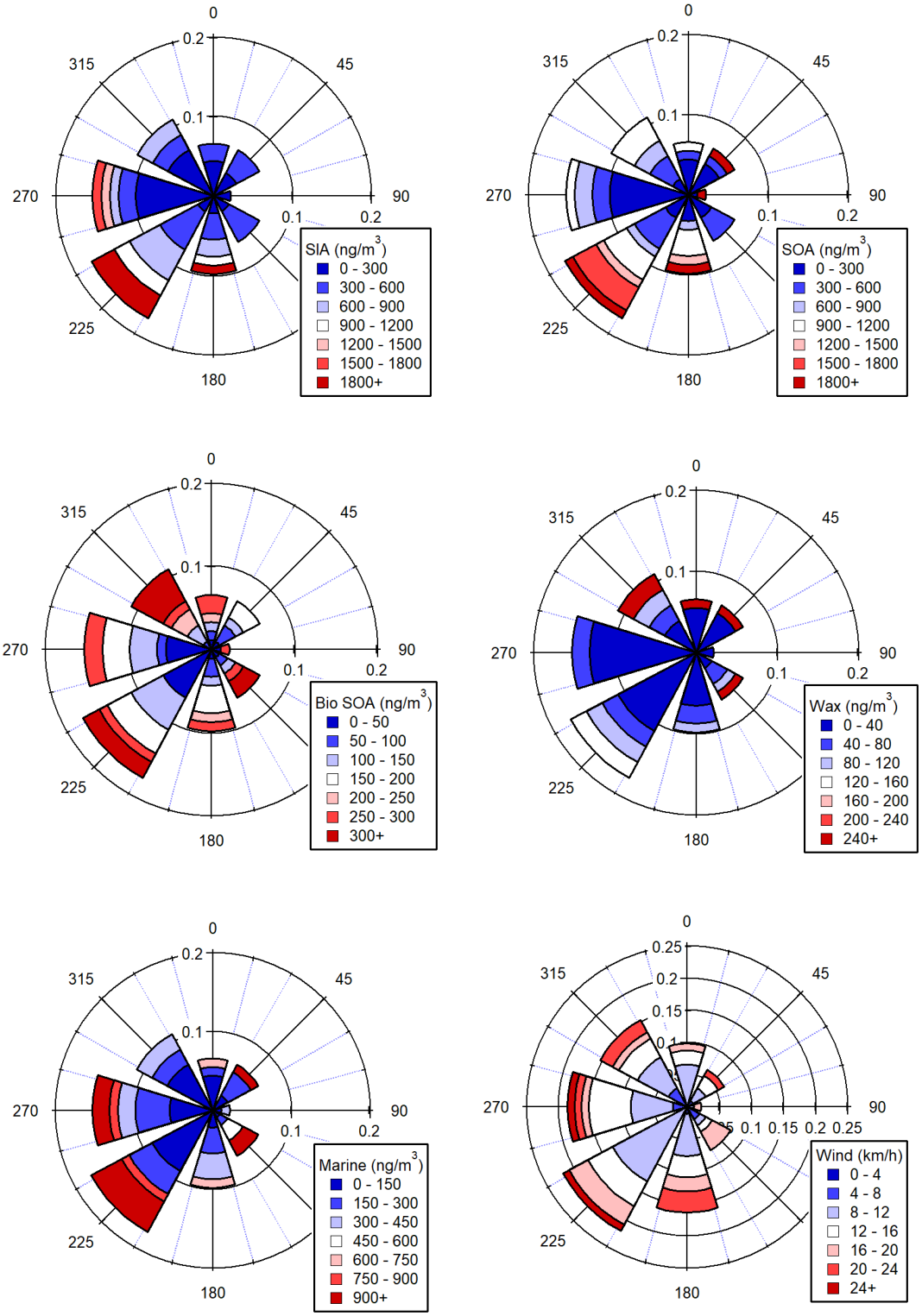

Fig. S10 (continued): Pollution rose plots for the PMF factors showing the frequency of a given concentration as function of wind direction.

References

Bray, E.E., Evans, E.D., 1961. Distribution of n-paraffins as a clue to recognition of source beds. Geochim. Cosmochim. Acta 22, 2–15. https://doi.org/10.1016/0016-7037(61)90069-2

Caumo, S., Bruns, R.E., Vasconcellos, P.C., 2020. Variation of the distribution of atmospheric n-alkanes emitted by different fuels' combustion. Atmos. 11, 1–19. https://doi.org/10.3390/atmos11060643

Calvo, A.I., Pont, V., Liousse, C., Dupré, B., Mariscal, A., Zouiten, C., Gardrat, E., Castera, P., Lacaux, C.G., Castro, A., Fraile, R., 2008. Chemical composition of urban aerosols in Toulouse, France during CAPITOUL experiment. Meteorol. Atmos. Phys. 102, 307–323. https://doi.org/10.1007/s00703-008-0319-2

Castro, L.M., Pio, C.A., Harrison, R.M., et al., 1999. Carbonaceous aerosol in urban and rural European atmospheres: estimation of secondary organic carbon concentrations. Atmos. Env. 33 (17), 2771-2781. https://doi.org/10.1016/S1352-2310(98)00331-8

Cesari, D., De Benedetto, G.E., Bonasoni, P., Busetto, M., Dinoi, A., Merico, E., Chirizzi, D., Cristofanelli, P., Donateo, A., Grasso, F.M., Marinoni, A., Pennetta, A., Contini, D., 2018. Seasonal variability of $PM_{2.5}$ and PM_{10} composition and sources in an urban background site in Southern Italy. Sci. Total Environ. 612, 202–213. https://doi.org/10.1016/j.scitotenv.2017.08.230

Cooper, J.E., Bray, E.E., 1963. A postulated role of fatty acids in petroleum formation. Geochim Cosmochim. Acta 27, 1113–1127. doi:10. 1016/0016-7037(63)90093-0

Esmaeilirad, S., Lai, A., Abbaszade, G., Schnelle-Kreis, J., Zimmermann, R., Uzu, G., Daellenbach, K., Canonaco, F., Hassankhany, H., Arhami, M., Baltensperger, U., Prévôt, A.S.H., Schauer, J.J., Jaffrezo, J.L., Hosseini, V., El Haddad, I. 2020. Source apportionment of fine particulate matter in a Middle Eastern Metropolis, Tehran-Iran, using PMF with organic and inorganic markers. Sci. Total Environ. 705, 135330. https://doi.org/10.1016/j.scitotenv.2019.135330.

Fadel, Marc, Ledoux, F., Farhat, M., Kfoury, A., Courcot, D., Afif, C., 2021. $PM_{2.5}$ characterization of primary and secondary organic aerosols in two urban-industrial areas in the East Mediterranean. J. Environ. Sci. (China) 101, 98–116. https://doi.org/10.1016/j.jes.2020.07.030

Fakhri, N., Fadel, M., Öztürk, F., Keleş, M., Iakovides, M., Pikridas, M., Abdallah, C., Karam, C., Sciare, J., Hayes, P.L., Afif, C., 2023. Comprehensive chemical characterization of PM2.5 in the large East Mediterranean-Middle East city of Beirut, Lebanon. J. Environ. Sci. 133, 118–137. https://doi.org/10.1016/j.jes.2022.07.010

Genga, A., Ielpo, P., Siciliano, T., Siciliano, M., 2017. Carbonaceous particles and aerosol mass closure in $PM_{2.5}$ collected in a port city. Atmos. Res. 183, 245–254. http://dx.doi.org/10.1016/j.atmosres.2016.08.022

Haque, M.M., Kawamura, K., Deshmukh, D.K., Fang, C., Song, W., Mengying, B., Zhang, Y.L., 2019. Characterization of organic aerosols from a Chinese megacity during winter: Predominance of fossil fuel combustion. Atmos. Chem. Phys. 19, 5147–5164. https://doi.org/10.5194/acp-19-5147-2019

Huang, X.H.H., Bian, Q., Ng, W.M., Louie, P.K.K., Yu, J.Z., 2014. Characterization of $PM_{2.5}$ major components and source investigation in suburban Hong Kong: A one year monitoring study. Aerosol Air Qual. Res. 14, 237–250. https://doi.org/10.4209/aaqr.2013.01.0020

Joseph, A.E., Unnikrishnan, S., Kumar, R., 2012. Chemical characterization and mass closure of fine aerosol for different land use patterns in Mumbai city. Aerosol Air Qual. Res. 12, 61–72. https://doi.org/10.4209/aaqr.2011.04.0049

Kang, M., Kim, K., Choi, N., Kim, Y.P., Lee, J.Y., 2020. Recent occurrence of PAHs and n-Alkanes in pm2.5 in Seoul, Korea and characteristics of their sources and toxicity. Int. J. Environ. Res. Public Health 17. https://doi.org/10.3390/ijerph17041397

Lee, E., Chan, C.K., Paatero, P., 1999. Application of positive matrix factorization in source apportionment of particulate pollutants in Hong Kong. Atmos. Environ. 33, 3201–3212. https://doi.org/10.1016/S1352-2310(99)00113-2

Li, W., Peng, Y., Bai, Z., 2010. Distributions and sources of n-alkanes in $PM_{2.5}$ at urban, industrial and coastal sites in Tianjin, China. J. Environ. Sci. 22, 1551–1557. https://doi.org/10.1016/S1001-0742(09)60288-6

Mason, B., Moore, C.B., 1982. Principles of Geochemistry, fourth edition. Wiley.

Meng, J., Martin, R. V., Li, C., van Donkelaar, A., Tzompa-Sosa, Z. A., Yue, X., Xu, J.-W., Weagle, C. L., and Burnett, R. T.: Source Contributions to Ambient Fine Particulate Matter for Canada, Environ. Sci. Technol., 53, 10269–10278, https://doi.org/10.1021/acs.est.9b02461, 2019.

Sciare, J., Oikonomou, K., Cachier, H., Mihalopoulos, N., Andreae, M.O., Maenhaut, W., et al., 2005. Aerosol mass closure and reconstruction of the light scattering coefficient over the Eastern Mediterranean Sea during the MINOS campaign. Atmos. Chem. Phys. Discuss. 5, 2427–2461. https://doi.org/10.5194/acp-5-2253-2005.

Schutgens, N. A. J., Gryspeerdt, E., Weigum, N., Tsyro, S., Goto, D., Schulz, M., and Stier, P. 2016. Will a perfect model agree with perfect observations? The impact of spatial sampling, Atmos. Chem. Phys., 16, 6335–6353, https://doi.org/10.5194/acp-16-6335-2016.

Shivani, Gadi, R., Sharma, S.K., Mandal, T.K., 2019. Seasonal variation, source apportionment and source attributed health risk of fine carbonaceous aerosols over National Capital Region, India. Chemosphere 237, 124500. https://doi.org/10.1016/j.chemosphere.2019.124500